Research Article

Immobilization of Retinoic Acid by Polyamino Acids: Lamellar-Structured Nanoparticles

Andreas F. Thnemann, Jochen Beyermann, Christian von Ferber, and Hartmut Lwen

Langmuir, **2000**, 16 (2), 850-857• DOI: 10.1021/la9906525 • Publication Date (Web): 14 October 1999

Immobilization of Retinoic Acid by Polyamino Acids: Lamellar-Structured Nanoparticles

Andreas F. Thünemann* and Jochen Beyermann

Max Planck Institute of Colloids and Interfaces, Am Mühlenberg, 14476 Golm, Germany

Christian von Ferber and Hartmut Löwen

Institut für Theoretische Physik II, Heinrich-Heine-Universität Düsseldorf, Universitätsstrasse 1, 40225 Düsseldorf, Germany

Received May 27, 1999. In Final Form: August 23, 1999

We discuss the preparation, the X-ray spectra and their theory, and electron microscopy of nanoparticles showing a lamellar internal structure. Retinoic acid was immobilized by complexation with poly(L-arginine), poly(L-histidine), and poly(L-lysine). The resulting solid-state complexes were prepared as nanoparticles with diameters of 320−380 nm, and with internal structures, which are smectic A-like. By small-angle X-ray scattering the unit cell was determined to be in the range of 3.10−3.62 nm, thus depending linearly on the monomer mass. The X-ray scattering of finite lamellar structures of "onion"- and "tart"-type spherical nanoparticles were determined theoretically. The uniform boundary of the onion-type particles results in secondary maxima near the Bragg reflections. Further, the highest degree of polydispersity to find these secondary maxima in scattering experiments was determined to be about 1% if the particle size is 300 nm. When electron microscopy was used, it was shown that the particles consist of a complex-containing core surrounded by a dispersing agent-containing shell. The core was revealed to be more of the tart- than the onion-type. When circular dichroism was used, the conformation of poly(L-arginine) and poly(L-lysine) within the complexes was determined to be an α-helix, whereas that of poly(L-histidine) was predominantly of the coil-type.

Introduction

Vitamin A and its analogues, in particular, retinoic acid, are involved in the proliferation and differentiation of epithelial tissues and have continued to be used in the treatment of dermatological disorders such as acne, psoriasis, and hyperkeratosis.[1,2] Currently, a lot of interest is being focused on how to understand the role of retinoic acid in cell differentiation. This is done by investigating the binding properties of retinoids on specific proteins,[3,4] its role in malignant-tumor inhibition,[5,6] and its regulation of brain functions.[7] Natural retinoids need to be bound to specific retinoic-binding proteins to ensure their protection, solubility, and transport by body fluids. Immobilization is a major problem in administering retinoic acid as a pharmacological agent. One way of achieving such immobilization and protection of retinoic acid is by binding it to a protein as it occurs in nature. A successful example for mimicking nature's strategy was shown by Zanotti[5] et al. when he cocrystallized transthyretin and retinoic acid. This, however, is a difficult and costly procedure. Recently, we have developed an easier and less expensive method for the required immobilization by the complexation of retinoic acid with synthetic cationic polyelectrolytes such as poly(ionene-6,3), poly(*N*-methylene-4-vinylene), and poly(diallyldimethylammonium).[8] The work presented here is on the immobilization of retinoic acid by three polyamino acids: poly(-L-lysine), poly(-L-arginine), and poly(-L-histidine). The mesomorphous structure of these complexes, which are prepared as nanoparticles, was examined.

Experimental Section

Materials. Crystalline all-trans retinoic acid (tretinoin, vitamin A acid) powder, 0.1 M hydrochloric acid and 0.1 M sodium hydroxide was purchased from Fluka. Poly(L-arginine hydrochloride) (M_v = 15 000−70 000), poly(L-histidine hydrochloride) M_v = 15 000−50 000), poly(L-lysine hydrobromide) (M_v = 15 000−30 000), 1-butanol (HPLC grade), and sodium hydroxide were obtained from Sigma-Aldrich. The Poloxamer 188 was a gift from ICI (Manchester, UK). All chemicals were used without further purification.

Complex Formation. Retinoic acid (100 mg) was dissolved in an aqueous sodium hydroxide solution at a pH of 8−9. Then, 2 mL of an equimolar amount of aqueous polyamino acid solution was adjusted to a pH of 8 and added in droplets while stirring. The stoichiometry of the complexes was calculated with respect to the charges. Complexes of the polyamino acids with retinoic acid were obtained immediately as yellow precipitates. After additional stirring for 15 min in the absence of light, the complexes were separated from the aqueous solution, washed with water (Millipore), and then dried in a vacuum. The elemental analysis obtained for poly(L-arginine) retinoate [observed (calculated for 1:1 stoichiometry)] was C 68.4 (68.2), H 8.7 (9.0), N 12.7 (12.2), Na < 0.1 (0), Cl < 0.1 (0); for poly(L-histidine) retinoate, C 70.4 (71.2), H 8.6 (8.2), N 9.7 (9.6), Na < 0.1 (0), Cl < 0.1 (0); and for poly(L-lysine) retinoate, C 71.3 (72.7), H 9.7 (9.5), N 6.3 (6.5), Na < 0.1 (0), Br < 0.1 (0). The complexes were dissolved in 2-butanol and cast on glass plates. The two-dimensional geometry of the films was stabilized by a glass frame, which was mounted on top of the glass sheet in the same way as that in the procedure described earlier.[9] After the evaporation of the solvent, the films

(1) Packer, L., Ed. *Methods in Enzymology*; Academic Press: San Diego, CA, 1990; Vol. 190.
(2) Lewin, A. H.; Bos, M. E.; Zusi, F. C.; Nair, X.; Whiting, G.; Bouquin, P.; Tetrault, G.; Carroll, F. I. *Pharm. Res.* **1994**, *11*, 192.
(3) Bourguet, W.; Ruff, M.; Chambon, P.; Gonemeyer, H.; Moras, D. *Nature* **1995**, *375*, 377.
(4) Lewin, A. H.; Bos, M. E.; Zusi, F. C.; Nair, X.; Whiting, G.; Bouquin, G. *Pharm. Res.* **1994**, *11*, 192.
(5) Zanotti, G.; D'Acunto, M. R.; Malpeli, G.; Folli, C.; Berni, R. *Eur. J. Biochem.* **1995**, *234*, 563.
(6) Jaeger, E. P.; Jurs, P. C.; Stouch, T. R. *Eur. J. Med. Chem.* **1993**, *28*, 275.
(7) Krezel, W.; Ghyselinck, N.; Samad, T. A.; Dupe, V.; Kastner, P.; Borelli, E.; Chambon, P. *Science* **1998**, *279*, 863.

10.1021/la9906525 CCC: $19.00
Published on Web 10/14/1999

could be easily removed. The thicknesses of the films used for measuring bulk properties were in the range of 0.1−1 mm.

Nanoparticle Formation. Dried complex films were powdered and a 1:1 mass ratio of Poloxamer 188 were mixed with a triturator. While the mixture was stirred and treated with ultrasound, water was added slowly until an opaque solution was obtained. The temperature was adjusted to a range between 20 and 26 °C. Finally, the mixture was purified by a 5-μm filter supplied by the Nalgene Co. The resulting dispersions where characterized by dynamic light scattering. The average particle sizes obtained were 320 nm for poly(L-arginine), 360 nm for poly(L-histidine), and 380 nm for poly(L-lysine) and had a polydispersity of about 0.2. The dispersed complexes were freeze-dried and later redispersed with water. After this procedure the particle sizes were increased up to values of about 400 nm and the polydispersities were about 0.3.

Methods. Circular dichroism was detected by a spectropolarimeter (J715 from Jas, Gross-Umstadt). The measurements were performed in the far-UV range (190−260 nm) on thin films on quartz plates and on complex solutions in 2-butanol. The anisotropic optical properties of complex films were examined by using a polarization microscope (Orthoplan-pol; Leitz) with an angle of 90° between the polarizer and analyzer. Wide-angle X-ray scattering (WAXS) measurements were carried out with a Nonius PDS120 powder diffractometer by transmission geometry. A FR590 generator was used as the source for Cu Kα radiation, monochromatization of the primary beam was achieved by means of a curved Ge crystal, and the scattered radiation was measured with a Nonius CPS120 position-sensitive detector. The resolution of this detector in 2θ was 0.018°. SAXS measurements were carried out with an X-ray vacuum camera with pinhole collimation (Anton Paar, Austria, model A-8054) equipped with image plates (type BAS III, Fuji). The image plates were read with a MAC Science Dip-Scanner IPR-420 and IP reader DIPR-420. Dynamic light scattering measurements were carried out with a submicron particle sizer, model 370 (Nicomp). Standard transmission electron microscopy (TEM) was performed on nanoparticles of the complexes coated with Poloxamer 188. Samples were prepared by pouring a droplet of 0.1% (w/w) aqueous dispersion onto a supporting grid. After the evaporation of the water, the samples were examined with a Zeiss EM 912 Omega TEM. Additional micrographs were taken, using freeze fractioning for sample preparation. A small amount of the sample was placed on a supporting disk, rapidly frozen in liquid propane, and cooled by liquid nitrogen. A freeze fracture apparatus BAF 400 (Balzers), equipped with an electron beam evaporator, was used for sample fractioning and replication. Freeze fractioning was carried out at −120 °C before Pt/C evaporation. The replicas were cleaned in sulfuric acid and demineralized water and then mounted on uncoated copper grids for further examination.

Results and Discussion

The retinaote **(1)** complexes of poly(L-arginine) **(2)**, poly(L-histidine) **(3)**, and poly(L-lysine) **(4)** were precipitated from aqueous solutions, purified, and cast to form films from complex solutions in 2-butanol. A sketch of the used compounds is shown in Figure 1. In comparison to complexes of retinoic acid with other polycations, such as poly(ionene-6,3), poly(*N*-methylene-4-vinylene), and poly(diallyldimethylammonium),[8] the dissolution rate of the polyamino acid complexes was significantly slower. In addition, complex films prepared from the former were flexible, had glass-transition temperatures in the range of −19 to 28 °C, and showed viscoelastic mechanical properties, whereas those of **(2)**, **(3)**, and **(4)** were brittle. No glass transition could be found by differential scanning calorimetry. The difference in the solubility and mechanical properties of retinoate complexes of polycations containing an atactic backbone and complexes with basic poly(L-amino) acids may be explained by the stereochemically unique polymer backbones of the latter, which enhanced the stiffness of the retinoate complex. It has already been stated that no glass transitions were found

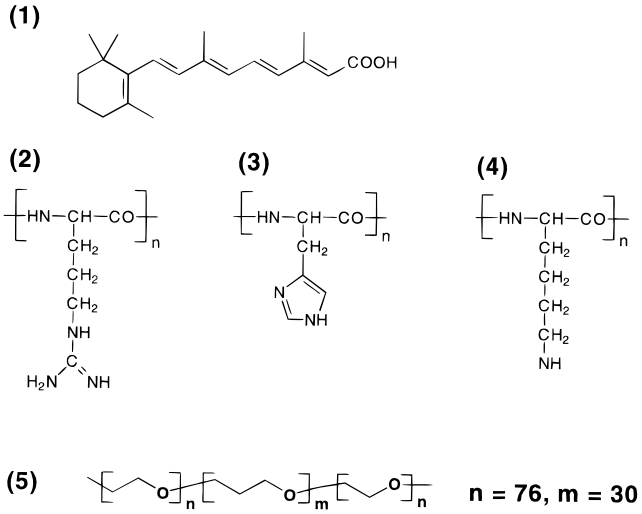

Figure 1. Substances used for complex formation and dispersion. **(1)** All-trans retinoic acid, **(2)** poly(-L-arginine), **(3)** poly(-L-histidine), and **(4)** poly(-L-lysine). As a dispersing agent, triblock copolymer **(5)** was used. It consisted of ethylene oxide and propylene oxide (Poloxamer 188).

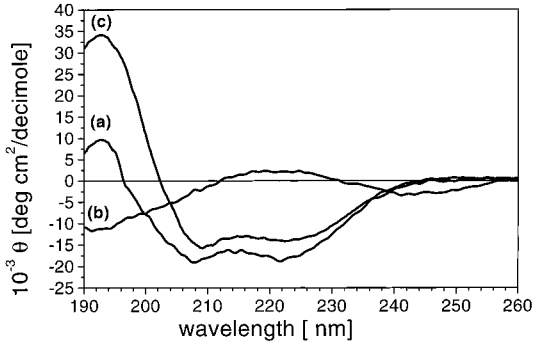

Figure 2. Circular dichroism spectra of poly(L-arginine) retinoate (a), poly(L-histidine) retinoate (b), and poly(L-lysine) retinoate (c). The complexes were prepared as films on quartz slides.

in solid-state complexes of poly(L-lysine) with alkyl sulfates[10] or soylecithin.[11] Therefore, at least for poly(L-lysine), the absence of a glass transition may be assumed to be a characteristic property of its solid-state complexes with amphiphiles.

Helix and Coil Conformations. The conformational state of the polymeric backbone of the complexes was examined by circular dichroism (CD). Figure 2 shows the CD spectra of complex films prepared on quartz slides. A maximum at 191 nm and two minima at 210 and 222 nm were found for poly(L-arginine) retinoate (curve (a) in Figure 2) and poly(L-lysine) retinoate (curve (c) in Figure 2). The spectra of complex solutions in 2-butanol showed the same characteristics. Therefore, we concluded that the conformation of the polymeric chains of both complexes in the solid and in solution of 2-butanol was an α-helix.[12,13] By contrast, a minimum at 193 nm and a maximum at 222 nm was observed in the CD spectrum of poly(L-

(8) Thünemann, A. *Langmuir* **1997**, *13*, 6040.
(9) Antonietti, M.; Conrad, J.; Thünemann, A. F. *Macromolecules* **1994**, *27*, 6007.
(10) Ponomarenko, E. A.; Tirrell, D. A.; MacKnight, W. J. *Macromolecules* **1998**, *31*, 1584.
(11) Wenzel, A.; Antonietti, M. *Adv. Mater.* **1997**, *9*, 487.
(12) Harada, A.; Cammas, S.; Kataoka, K. *Macromolecules* **1996**, *29*, 6183.
(13) Bradbury, E. M.; Crane-Robinson, C.; Goldman H.; Rattle, H. W. E. *Biopolymers* **1998**, *6*, 851.

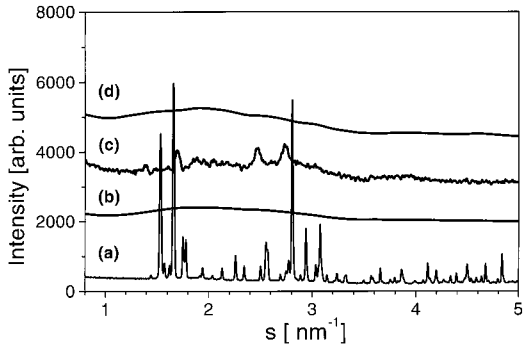

Figure 3. Wide-angle X-ray diagrams of crystalline all-trans retinoic acid (curve (a)) and its complexes with polyamino acids. In the curve of poly(L-arginine) retinoate and poly(L-lysine) retinoate (curves (b) and (d), respectively) no crystalline reflections were found. However, three weak crystalline reflections are present in the curve of poly(L-histidine) retinoate at $s = 1.69$, 2.48, and 2.73 nm^{-1} (curve (c)). This is indicative of a partially crystalline complex structure. The scattering vector is defined as $s = 2/\lambda \sin \theta$.

histidine) retinoate (curve (b) in Figure 2). This proves that there was a predominantly coil conformation for poly(L-histidine) retinoate. Because the pK_a of the imidazole group of histidine residues was around 6.6,[14] the uncharged forms of histidine were present at the complex preparation condition (pH 9). By contrast the poly(L-arginine) and poly(L-Lysine) were charged at pH 9. The pK_a values of the basic groups were 12.48 and 10.53, respectively.[15] On the basis of these data, it may be assumed that the charging of the polyamino acid leads to an α-helix conformation of the complex.

Molecular Organization. Information about the molecular packing of the retinoate moieties was obtained by wide-angle X-ray scattering (WAXS). The WAXS pattern of retinoic acid (curve (a) in Figure 3) is characterized by a number of sharp reflections resulting from the high degree of crystallinity. Retinoic acid crystallizes in two similar crystalline modifications (triclinic and monoclinic),[16] which led to the reflex pattern observed. As shown in Figure 3, curves (b) and (d), the crystallinity of retinoic acid was prevented by complexation with poly(L-arginine) and poly(L-lysine). As is the case in complexes with poly(diallyldimethylammonium chloride), ionene-3,6, and poly(*N*-methyl-4-vinylpyridine),[8] the maximum of the broad wide-angle reflection corresponds to a Bragg spacing of 0.52 nm. The absence of sharp reflections in the wide-angle region proves the lack of crystallinity. Again, the properties of poly(L-histidine) retinoate differ from that of the others. Weak but significant reflections at $s = 1.69$, 2.48, and 2.73 nm^{-1} were observed which are indicative for the partial crystallinity of the complex (curve (c) in Figure 3). The scattering patterns remained constant for several months, and therefore it is assumed that the complexes are very likely to be thermodynamically stable. The absence of crystallinity is an interesting aspect, both from a material science and a pharmaceutical point of view, because the weight percentage of the crystallizable retinoic molecules in all complexes is about 70%. The strong reduction of crystallinity may be explained as follows: To maintain electrostatic neutrality, any diffusion of retinoic moieties must be accompanied by a correlated movement of charged polymer chains, such that no phase separation, and consequently no crystallization, can occur.

Supramolecular Structures. In an earlier work we reported on lamellar mesomorphous retinoate complex structures[8] and it was expected that the retinoate complexes of **(2)**, **(3)**, and **(4)** form similar mesophases. The films of all complexes are optically anisotropic, as was found during examination between crossed polarizers. An example of the optical textures is shown in Figure 4. Obviously, the complexes are mesomorphous, but an unambiguous identification of the mesophases on the basis of the optical properties was not possible. Therefore, the state of order on a length scale of several nanometers was investigated by small-angle X-ray scattering measurements, carried out on freeze-dried complex nanodispersions. Aqueous nanodispersions were prepared from complex powder with the aid of Poloxamer 188, a triblock copolymer, consisting of two poly(ethylene oxide) blocks and a polypropyleneoxide (see Figure 1). Poloxamer 188 is a common nonionic surfactant frequently used as a steric stabilizer in pharmaceuticals and proved to be capable of stabilizing nanoparticles.[17−19] The size of the complex particles as determined by dynamic light scattering was in the range of 300−380 nm in diameter with a polydispersity of about 0.20. It was found that the complex dispersions could be redispersed after freeze-drying. As a result of this procedure the particle sizes increased slightly to about 400 nm and the polydispersity increased to values of about 0.3. The simplicity of the preparation of these nanoparticles seems to be an attractive feature of the complexes. Recently, we reported on a polyelectrolyte−fluorosurfactant complex, which can form nanoparticles with an internal mesomorphous structure.[20] As in these complexes, in the small-angle X-ray scattering diagrams of nanodispersions of retinoate complexes equidistant reflections were also present (see Figure 5). It can be seen that the positions and the sharpness of the scattering peaks are different for the three complexes. In the case of poly(L-arginine) retinoate a lamellar repeat unit of 3.62 nm was determined by fitting a Lorentzian peak profile onto the (001) reflection. The corresponding values for poly(L-histidine) and poly(L-lysine) were 3.27 and 3.10 nm, respectively. Obviously the size of the repeat unit increased with an increasing mass of the monomer. In addition, the increase of the size of the repeat unit is linear with respect to the mass of the monomer unit (+0.0185 nm/mass unit). This linear scaling is indicative of the smectic A-like structures of the three complexes.

The correlation lengths of the structures were determined from the reciprocal width of the reflections; they were 27 ± 1, 15 ± 3, and 38 ± 1 nm (arginine, histidine, and lysine). The correlation length values can be explained by an increasing stacking order of the smectic layers from poly(L-histidine) retinoate, poly(L-arginine) retinoate, to poly(L-lysine) retinoate. Such differences may be the result of packing constraints due to their different molecular geometries, which may lead to different degrees of frustrations.[9] To our knowledge this is the first report on organic nanoparticles with a smectic A-like ordering, whereas inorganic materials with complex forms such as mesoporous silica have become a topic of intense research activity.[21,22] The question arises on how to characterize

(14) Botelho, L. H.; Gurd, F. R. N. *Handbook of Biochemistry and Molecular Biology*, 3rd ed.; Fasman, G. D., Ed.; CRC Press: Cleveland, 1976; Vol. 2, p 689.
(15) Lide, D. R., Ed. *Handbook of Chemistry and Physics*, 73rd ed.; CRC Press: Boca Raton, FL, 1992.
(16) Stam, C. H. *Acta Crystallogr.* **1972**, *28*, 2936.
(17) Douglas S. J.; Davis S. S. *J. Colloid Interface Sci.* **1985**, *103*, 154.
(18) Lechmann, T.; Reinhart, W. H. *Clin. Hemorheol.* **1998**, *18*, 31.
(19) Pons, M.; Garcia, M. L.; Valls, O. *Colloid Polym. Sci.* **1991**, *269*, 855.
(20) Thünemann, A. F.; Lieske, A.; Paulke B.-R. *Adv. Mater.* **1999**, *11*, 321.
(21) Mann S.; Ozin, G. A. *Nature* **1996**, *382*, 313.

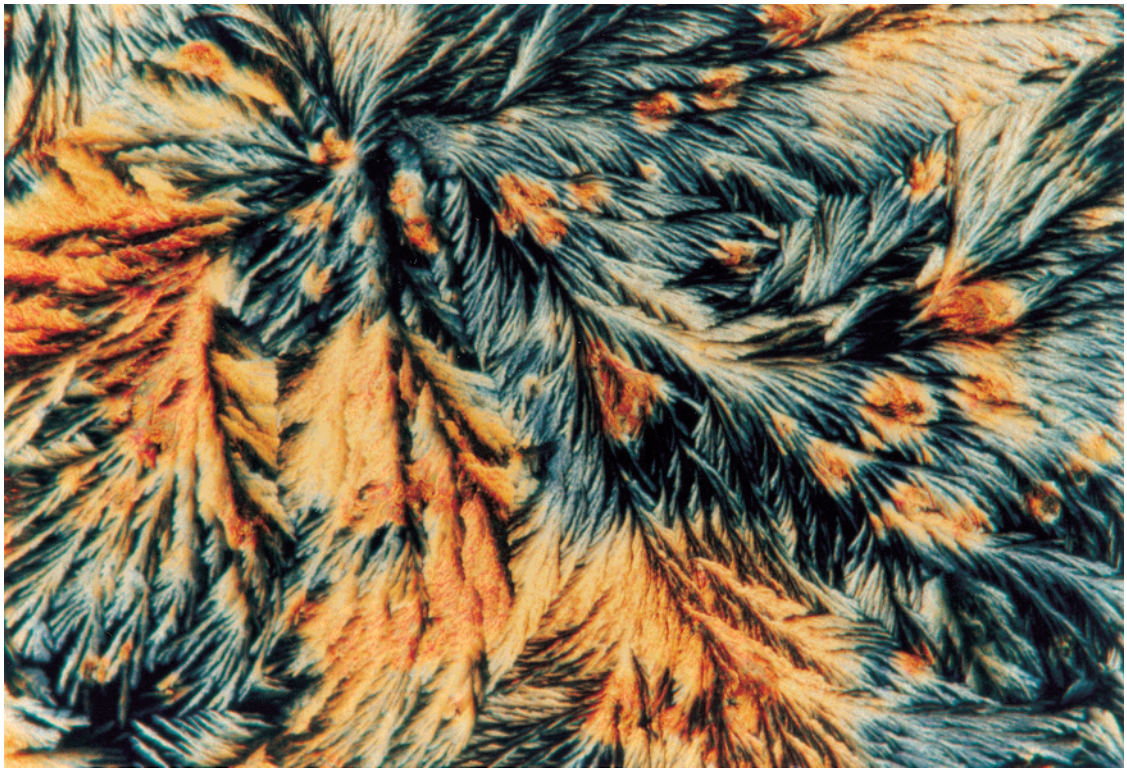

Figure 4. Polarization micrograph of poly(L-arginine) retinoate prepared as a film (magnification is 100).

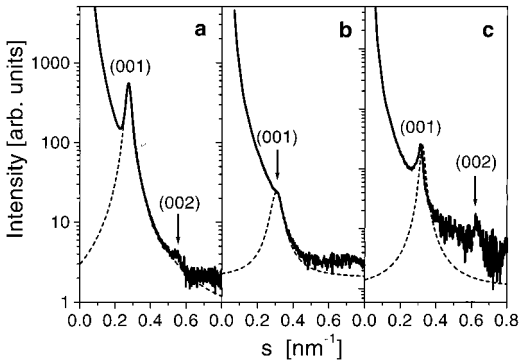

Figure 5. Small-angle X-ray scattering curves of poly(L-arginine) retinoate (a), poly(L-histidine) retinoate (b), and poly-(L-lysine) retinoate (c). The dashed lines are fits using a Lorentzian peak profile. Repeat units are 3.62, 3.27, and 3.10 nm.

the internal lamellar particle structure in detail. Parameters which are easily available are only the size of the particles and the size of the repeat unit within them. In earlier works on polyelectrolyte surfactant complex films, it was found that a good model for the description of their mesophase structures could be made by the microphase separation of the ionic-rich and hydrophobic-rich regions. Often, the density transition between these regions is given by a step function, which is similar to that found for strong segregated block copolymers and can be identified by the presence of Porod's law.[23] With such ideal phase-separated lamellar sheets within the complex nanoparticles, we assume two limiting cases for their internal structures: an "onion"- and "tart"-like structure. A sketch of the cross sections through such particles with a finite lamellar structure is shown in Figure 6. An adequate method for

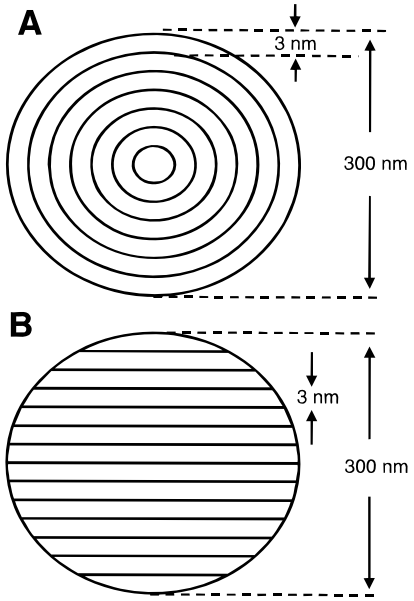

Figure 6. Idealized models for the finite lamellar structures of complex nanoparticles are the onion-like (A) and the tart-like structures (B). The size of the particles is about 300 nm whereas the internal lamellar structure has a unit cell dimension of about 3 nm.

their investigation is high-resolution small-angle X-ray or neutron scattering.

Scattering by Finite Lamellar Structures of Onion- and Tart-Type Particles. To discriminate between different mesomorphous-structured nanoparticles, we will discuss the X-ray scattering intensities for spheres with an internal lamellar structure. In particular, we will look for indicators which distinguish an onion-type structure of concentric lamellae (Figure 6, curve A) from a structure of parallel layers (Figure 6, curve B). This object will be called a tart-type. Other structures may be constructed

(22) Huo, Q.; Feng, J.; Schüth, F., Stucky, G. D. *Chem. Mater.* **1997**, *9*, 14.
(23) Micha, M. A.; Burger, C.; Antonietti, M. *Macromolecules* **1998**, *31*, 5930.

by the superposition of these limiting cases, which then will look more like "patch-work". We assume the electron density $\rho(r)$ is given and calculate the scattering amplitude $A(s)$ as a Fourier transform of $\rho(r)$. Here, the scattering vector is defined as $s = (2/\lambda) \sin \theta$. When the scattering is due to a spherically symmetric structure such as that of the onion-type, the scattering amplitude is a function of the absolute value of s only. In the case of the tart-type structure we assume that we scatter from an ensemble of arbitrarily oriented spheres. Then, the total intensity is a sum over all orientations and again a function of s only. For the onion structure we calculate the scattering intensity as $I(s) = |A(s)|^2$. Theoretical descriptions of mesophases as disordered extended lamellar structured are described earlier, for example, by Ruland et al.,[24] Richter et al.,[25] and Hosemann et al.[26,27]

Concentric Lamellae: Onion-Type. The scattering amplitude for a spherically symmetric electron density $\rho(r)$ may be written as

$$A(s) = 4\pi \int_0^\infty \rho(r) \frac{\sin(2\pi rs)}{2\pi rs} r^2 \, dr \tag{1}$$

We assume a sphere of diameter $D = 2R$ with layer boundaries at $0 = r_0 < r_1 < r_2 < \ldots < r_n = R$ and layer densities $\rho_1, \ldots, \rho_n$. The function $\rho(r)$ then becomes

$$\rho(r) = \begin{cases} \rho_j & r_{j-1} \le r \le r_j \\ 0 & r \ge r_n \end{cases} \tag{2}$$

The scattering amplitude for such a structure is given analytically as a sum of the amplitudes $\Phi(x)$ of the spheres[28]

$$A(s) = \frac{3}{(2\pi Rs)} \sum (\Phi(2\pi r_j s) - \Phi(2\pi r_{j-1} s))\rho_j$$

with

$$\Phi(x) = \sin(x) - x \cos(x) \tag{3}$$

Here, we have normalized $A(s)$ such that $A(0) = 1$ for a sphere of constant unit density $\rho_1 = \rho_2 = \ldots \rho_n = 1$. In our numerical study we calculate the corresponding intensities $I(s)$ for spheres of $n = 100$ and alternating layers of thicknesses d_1 and d_2 with respective densities $\rho^{(1)}$ and $\rho^{(2)}$. The above sum is then evaluated with corresponding values for the even and odd integers $j = 2m$ and $j = 2m + 1$. We insert $r_{2m} = 2mR/n$ and $r_{2m+1} = r_{2m} + d_1$ using densities $\rho_{2m} = \rho^{(2)}$ and $\rho_{2m+1} = \rho^{(1)}$.

Cylinder Symmetry: Tarts. Scattering from spheres with an internal structure of parallel lamellae (Figure 6b) needs a slightly different approach because of the reduced symmetry of the structure. The scattering amplitude for a single such sphere depends on the angle ϑ between the wave vector **s** and the symmetry z-axis of the sphere. We use cylinder coordinates (z,r,ϕ) and describe the contour of the sphere as $r(z) = (R^2 - z^2)^{1/2}$. The electron density is now a function of the z-coordinate only, $\rho(z)$. The scattering amplitude is given by the following Fourier integral:

$$A(s,\vartheta) = \frac{1}{R^3} \int_{-R}^{R} dz \rho(z) \int_{-r(z)}^{r(z)} dr' \int_0^{2\pi} d\phi \times \exp i(2\pi srz \cos \vartheta + 2\pi sr' \sin \vartheta \cos \phi)$$

$$= \frac{1}{R^3} \int_{-R}^{R} dz \rho(z) \frac{r(z)}{2\pi s \sin \vartheta} J_1(2\pi sr(z) \sin\vartheta) \times \exp(i2\pi sz \cos \vartheta) \tag{4}$$

Here, the ϕ and r' integrations were reduced to the Bessel function $J_1(x)$.[29] We again assume a sphere of diameter $D = 2R$ with layer boundaries at $-R = z_0 < z_2 < \ldots < z_n = R$ and layer densities $\rho_1, \ldots, \rho_n$. The function $\rho(z)$ then becomes

$$\rho(z) = \begin{cases} \rho_j & z_{j-1} \le z \le z_j \\ 0 & |z| \ge R \end{cases} \tag{5}$$

In a first approximation one may assume a constant radius $r(z) = r(z_i)$ in each layer j. This approximates the sphere by a pile of n cylinders. Then, the scattering amplitude is again simply given by the sum

$$A_{\text{app}}(s,\vartheta) = \frac{1}{R^3 (2\pi s)^2 \sin \vartheta \cos \vartheta} \times \sum_{j=1}^{n} \rho_j r(z_j) J_1(2\pi r(z_i) \sin \vartheta)(e^{(2\pi i z_j s \cos \vartheta)} - e^{(2\pi i z_{j-1} s \cos \vartheta)}) \tag{6}$$

While this approximation is already rather good (with an error of ~5% in our case), we chose to perform the evaluation of eq 4 by more refined numerical integration.

The scattering intensity results from an integration over all orientations of these tart-type particles:

$$I(s) = \frac{1}{2} \int_0^\pi d\vartheta \sin \vartheta |A(s,\vartheta)|^2 \tag{7}$$

To match the onion-layered systems described above, we calculated the corresponding intensities *I(s)* for spheres with $n = 200$ alternating layers of thickness d_1 and d_2 with respective densities $\rho^{(1)}$ and $\rho^{(2)}$. The integral or sum was then evaluated by inserting $z_{2m} = 2mD/n$ and $z_{2m+1} = z_{2m} + d_2$ for the even and odd values of j, again using densities $\rho_{2m} = \rho^{(2)}$ and $\rho_{2m+1} = \rho^{(2)}$.

Comparison of Onion-Type and Tart-Type. To produce results that allow for a comparison of the two limiting internal structures for a lamellar sphere, we calculated the spectrum of intensities for model systems using realistic data. The two parameters that were taken were the ratio of the two densities $\rho^{(1)}/\rho^{(2)}$ and the ratio of the thickness d_1 of the first part of the double layer to its total thickness $d = d_1 + d_2$. The parameter d_1 is interpreted here as the thickness of the nonionic, retinoate rich phase and d_2 as the thickness of the ionic, the polyelectrolyte-rich phase. We consider two complexes C1 and C2 with differing parameter values. For the complex C1 we have for the densities $\rho^{(1)}/\rho^{(2)} = 0.9/1.1$ and for the layer thickness $d_1/d = 1.80/3.00$. For the other complex we consider, C2, these numbers are 0.9/1.1 and 2.07/3.00, respectively. Figure 7 shows the logarithmic intensities for complex C1 in simultaneous plots for the onion-type and tart-type structures. The main peaks in intensity correspond to integer values of $m = sd$. For C1 the peak

(24) Wolf, T.; Burger, C.; Ruland, W. *Macromolecules* **1994**, *27*, 3301.
(25) Richter, D.; Schneiders, D.; Monkenbusch, M.; Willner, L.; Fetters, L. J.; Huang, J. S.; Lin, M.; Mortensen, K.; Farago, B. *Macromolecules* **1997**, *30*, 1053.
(26) Hosemann, R.; Hindeleh, A. M. *J. Macromol. Sci.-Phys.* **1995**, *B34*, 327.
(27) Hosemann, R.; Bagchi, S. N. *Direct Analysis of Diffraction by Matter*; North-Holland Publ. Co.: Amsterdam, 1962.
(28) Glatter, O. *Small Angle X-ray Scattering*; Academic Press: London, 1982.
(29) Gradshtein, I. S.; Ryzhik, I. M. *Table of Integrals, Series and Products*; Academic Press: London, 1995.

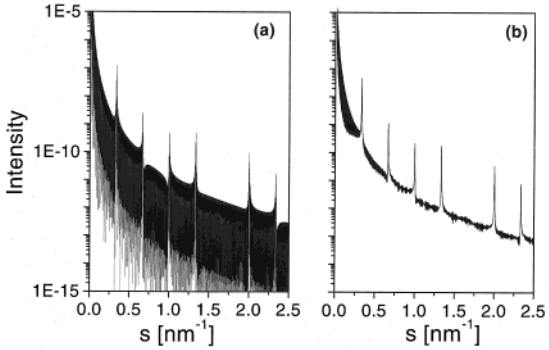

Figure 7. Theoretical scattering curves of lamellar nanoparticles with an onion-type structure (a) and a tart-type structure (b). The lamellar unit cell dimension is $d = 3.00$ nm and $d_1 = 1.80$ nm. Densities are $\rho_1 = 0.9$ and $\rho_2 = 1.1$. The size of the particle is $100d = 300$ nm. The density of the surroundings is 1.

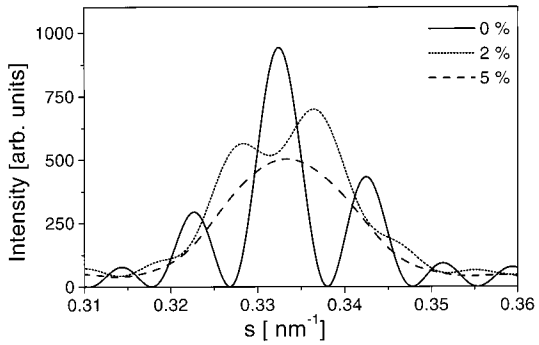

Figure 8. Theoretical scattering curves of lamellar nanoparticles with an onion-type structure of 20 layers and different degrees of polydispersity in the region of the first Bragg reflection. The lamellar unit cell dimension is $d = 3.00$ nm and $d_1 = 1.80$ nm. Densities are $\rho_1 = 0.9$ and $\rho_2 = 1.1$. The size of the particle is $100d = 300$ nm. The density of the surroundings is 1.

at $m = 5$ is missing. The reason is that here $d_1/d = 3/5$ and cancellation takes place in both sublayers individually for $m = 5$. The fine structure of the curves can be shown to result from the overall dimensions of the spheres, i.e., from integer values of sD. Obviously, this fine structure is a lot more pronounced in the case of the spherically symmetric onion structure. This difference results from the spherical symmetry and the uniform boundaries of the onion and, in principle, makes it possible to distinguish onion-type and tart-type structures by small-angle X-ray scattering experiments. Note that in the logarithmic plot values close to zero also become pronounced. No significance can be given to the amplitudes of these downward "peaks" because they have an artificial distribution due to the numerical cutoff. To study the difference of the two internal structures in more detail, we displayed the intensities near the first peak at $s = 1/d$ in linear plots (Figures 8, 9a, and 9b). In addition we considered whether the apparent difference in the signal may indeed be detected in a realistic experiment. To this end, we allowed for a polydispersity of the diameter D of the onions to a value of 1%. In our model this means a deviation of up to ± 1 layer. The intensity for scattering from such a polydisperse sample, we calculate by averaging over intensities I_D for onions with diameter D in the range $D_0 \pm 1\%$, assuming a uniform distribution for D. An onion for which the diameter D is not an integer multiple of the layer thickness d, we allow to have a core layer that is smaller than d. The intensity resulting from this average is plotted together with the original curves in Figure 9.

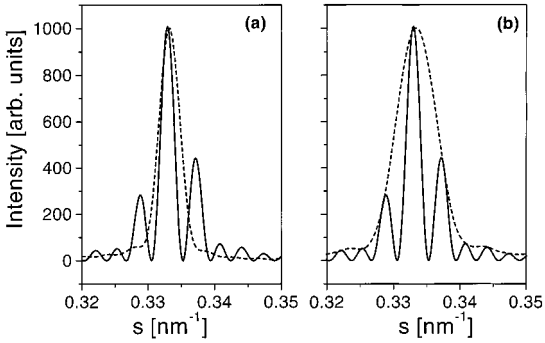

Figure 9. Scattering in the region of the first Bragg reflection. The scattering of the onion-type particle is characterized by a number of additional maxima (diagram (a), solid line). By contrast, no additional maxima are present in the scattering of the tart-type particle (diagram (a), dashed line). A polydispersity of 1% smears out the additional maxima ((b), dashed line), but these are present in the scattering of the onion-type particle ((b), solid line). The particle parameters are $d = 3.00$ nm, $d_1 = 1.80$ nm, $\rho_1 = 0.9$, $\rho_2 = 1.1$, and $D = 100d$.

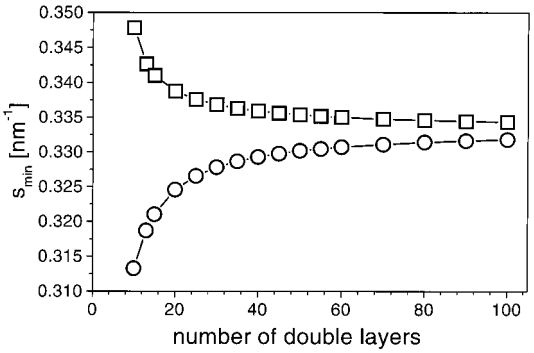

Figure 10. Positions of the two minima next to the first Bragg reflection. The particle parameters are $d = 3.00$ nm, $d_1 = 1.80$ nm, $\rho_1 = 0.9$, $\rho_2 = 1.1$, and $D =$ (number of layers) $\times$ d.

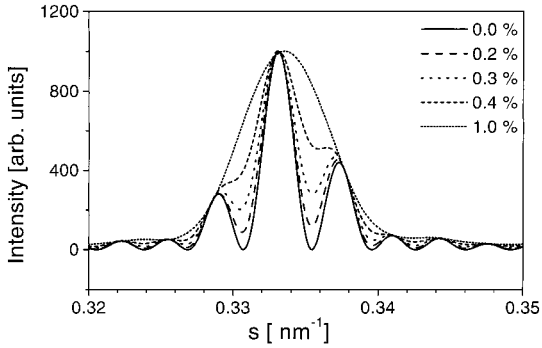

Figure 11. SAXS: Influence of the polydispersity for onion-type particles. The particle parameters are $d = 3.00$ nm, $d_1 = 1.80$ nm, $\rho_1 = 0.9$, $\rho_2 = 1.1$, and $D = 100d$.

Obviously, polydispersity smears out the fine structure of the onion-type signal, but a slight yet significant difference to the tart-type signal remains. From the width of the Bragg reflection a correlation length of about the size of the particle (300 nm) was determined. This is an order of magnitude larger than those observed. It must be stated that currently the polydispersity (20%) of the complex nanoparticles is too large to obtain detailed information by small-angle X-ray scattering. It will become easier to detect the onion-type scattering experimentally when the particle size decreases. In this case the distance between the minima next to the Bragg peak (see Figure 9) increases. This is clearly shown in Figure 10. The influence of the polydispersity on the scattering curve is demonstrated in

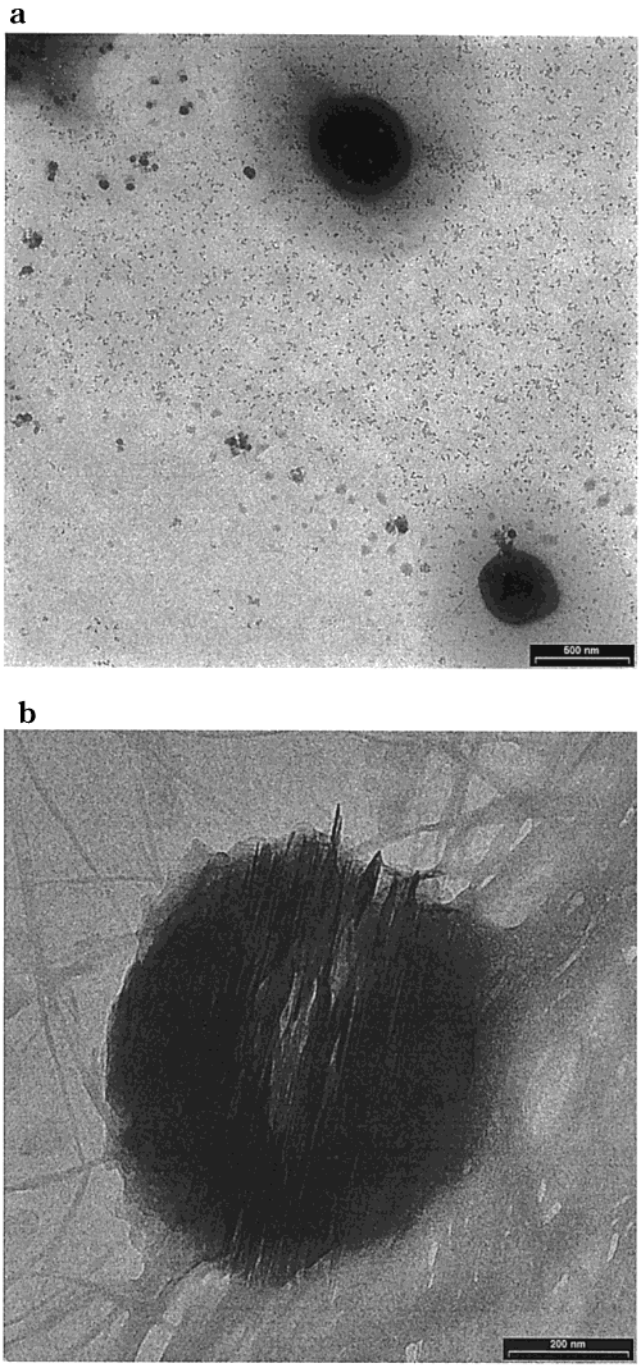

Figure 12. Typical TEM pictures of a dried dispersion on a copper grid. (a) At lower resolution spherical complex particles are shown surrounded by a halo consisting of block copolymers (scale bar = 500 nm). (b) At higher resolution, the internal structure of the particle is revealed to be tart-like (scale bar = 200 nm).

Figure 11. It seems to be realistic to think that we will be able to detect onion-type structures experimentally if the number of double layers is not greater than 20 and the polydispersity is lower than 5% (see Figure 8).

Electron Microscopy. For more insight into the internal particle structure, even for larger polydispersity, electron microscopy experiments were carried out. In TEM pictures of dried complex nanoparticle dispersions (Figure 12 a) it can be seen that the nanoparticles consist of a core with a high contrast, which is surrounded by a shell of lower contrast. We believe the core consists of the complex and the shell of the dispersing agent, Poloxamer 188. At

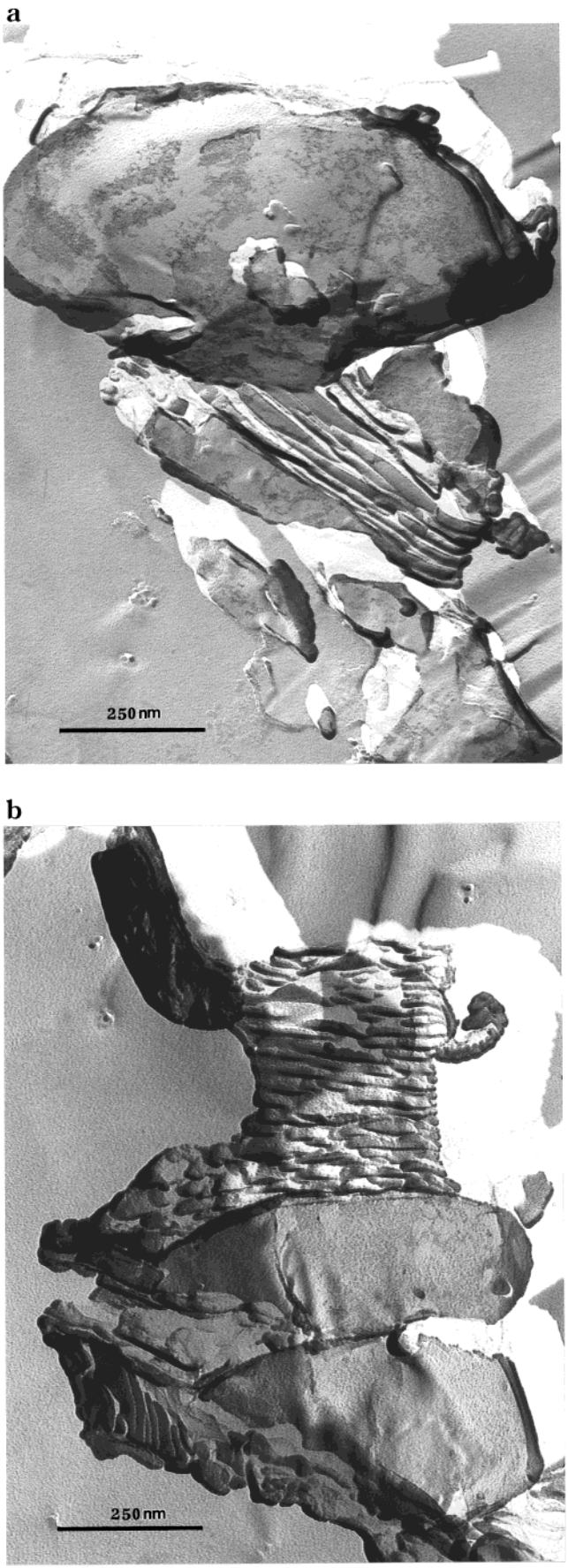

Figure 13. Freeze fracture TEM pictures of an aqueous poly-(L-arginine) retinoate complex dispersion.

a higher resolution (Figure 12b) it can be seen that the internal structure of a dried particle is split into discrete layers, extending form one side of the particle to the other. This is very much indicative of a more tart-type particle structure. In further experiments freeze-fractured particles were investigated. As can be seen from the example in Figure 13a,b, lamellar structures of about 60% of the particle sizes without any significant curvature were observed. Therefore, on the basis of electron microscopy data it seems to be very likely that the kind of finite lamellar particle structure is much more tart-type than onion-type. As has been the case in small-angle X-ray investigations currently being undertaken, we were not able to determine the values of d_1 and d_2 by electron microscopy. The reason for the formation of the tart-type particles is not understood yet but may be due to their preparation from films. In films the lamellar domain size is likely to be much larger than the size of the nanoparticles and tart-type.

Conclusion

We have shown that the solid-state complexes formed by poly(L-arginine), poly(L-histidine), and poly(L-lysine) cations and retinoic acid can be prepared as films and nanoparticles. The high content of retinoate moieties, the absence of crystallinity, and low particle sizes could make these complexes interesting as a new carrier for the delivery of retinoic acid, either transdermal or in body fluids. It may be speculated that supramolecular structures such as the smectic A-like nanoparticles of the tart-type presented here can lead to interesting release profiles of pharmaceutically active agents.

Acknowledgment. The authors would like to thank J. Hartmann for performing the electron microscopy measurements, E. Vieira for help in measuring circular dichroism, C. Burger for a discussion of the X-ray data, and the Max-Planck Society for their financial support.

LA9906525